

Article

# Selective Flotation of Pyrite from Arsenopyrite by Low Temperature Oxygen Plasma Pre-Treatment

Jincheng Ran <sup>1,2,3,\*</sup>, Xianyang Qiu <sup>2,3</sup>, Zhen Hu <sup>2,3</sup>, Quanjun Liu <sup>1</sup> and Baoxu Song <sup>2,3</sup>

<sup>1</sup> State Key Laboratory of Complex Non-ferrous Metal Resources Clean Utilization, Kunming University of Science and Technology, Kunming 650093, China; kmlqj@sina.com

<sup>2</sup> Guangdong Institute of Resources Comprehensive Utilization, Guangzhou 510650, China; qxysy@163.com (X.Q.); gzyxks123@163.com (Z.H.); winsbx@163.com (B.S.)

<sup>3</sup> Guangdong Provincial Key Laboratory of Development and Comprehensive Utilization of Mineral Resources, Guangzhou 510650, China

\* Correspondence: rjc@kmust.edu.cn

Received: 17 October 2018; Accepted: 30 November 2018; Published: 4 December 2018



**Abstract:** In this study, the surface modification of arsenopyrite and pyrite with low temperature oxygen plasma was developed as an effective approach to improve the flotation separation efficiency of minerals. The micro-flotation experiments results indicated that plasma pre-treatment can achieve selective flotation of arsenopyrite from pyrite. The XPS analysis results indicated that the oxidation degree of plasma-modification arsenopyrite surface is much higher than that of pyrite. A large number of sulfide components on the surface of the mineral were oxidized to highly-valence hydrophilic oxides by plasma pre-treatment. ICP-MS analysis results revealed that the dissolution rate was determined by the oxidation degree of minerals and plasma modified accelerated the dissolution of arsenopyrite and pyrite. Zeta potential determination results confirmed that plasma can keep a relatively higher adsorption of SBX on the pyrite surface but inhibit the adsorption of collector onto the arsenopyrite surface.

**Keywords:** low temperature oxygen plasma; arsenopyrite; pyrite; surface modification; flotation

## 1. Introduction

Pyrite has been a vital mineral source to produce sulfur acid, a considerable amount of pyrite is closely associated with arsenopyrite [1]. Separation or selective depression of arsenopyrite from pyrite becomes imperative, especially extraction of the gold or silver associated with the pyrite matrix. In addition, when arsenic-bearing pyrite concentrate is smelted, hydrogen arsenide, arsenite and organic arsenide will be produced, posing a serious threat to the environment [2,3]. Given the strict requirements for arsenic content in pyrite concentrate, higher separation efficiency of pyrite and arsenopyrite is of more significance. Separation of arsenopyrite from pyrite is usually achieved by selective depression of arsenopyrite using depressants like cyanide or oxidizing agents (e.g., hydrogen peroxide and magnesia-ammonia mixture) to selectively oxidize arsenopyrite [3–5]. As arsenopyrite is more sensitive to oxidation than pyrite, the floatability of arsenopyrite is reduced by controlling the concentrations of the depressants and collectors and the flotation parameters [5]. The hydrophilic iron hydroxyl compounds and the arsenate preferentially precipitate on the arsenopyrite surface by drawing upon the difference in oxidation rate, while pyrite still maintains a high recovery [6,7].

However, as the physical and chemical properties of arsenopyrite are similar to those of pyrite, arsenopyrite presents a similar hydrophobicity with pyrite in the flotation process when xanthate serves as collector [8,9]. As their hydrophobic surface species are dixanthogen, xanthates are not cation-selective in the case of separation of arsenopyrite and pyrite, which makes it very difficult by

flotation separation [10,11]. No matter what type of depressant is applied, it can also depress pyrite and arsenopyrite simultaneously [12]. Moreover, the floatability of pyrite will also be significantly reduced when the flotation proceeds in a high alkali pulp [13,14]. Furthermore, the conventional arsenopyrite depressants such as cyanide and potassium permanganate are harmful to human health and environment, which limits the application of reagents in flotation separation. Since flotation selectivity and separation efficiency are dependent on the reagent concentrations, pulp redox potential and slurry pH in the conditioning stage, rigorously controlling of these parameters is also considered necessary for the prevention of depressing the pyrite [3].

Low temperature plasma has been proven as an effective and powerful method in surface modification of organic and inorganic materials [15,16]. Low temperature plasma is formed by introducing electric energy to the gas, causing the breakdown of the gas into ions and electrons [17]. It is a collection of positively and negatively charged particles and neutral species, consisting of electrons, ions, neutral atoms, molecules and large numbers of other species (e.g., excited species and various radicals) [18]. The electrons and ions have abundant high energy to activate the gas and create reactive species by electron impact excitation, ionization, dissociation and attachment, which can break the chemical bonds on the material surfaces and form new bonds [19]. When the materials are put into the low temperature plasma, energy exchange, charge transfer, molecular decomposition or recombination and electron adsorption will be resulted in by the reactive species collide with the material surfaces, causing physical or chemical reactions on the surface of the materials to achieve the surface modification of the materials [18]. Compared with flotation reagents, surface modification of minerals by low temperature plasma has the advantages of pollution-free and completely controllable process conditions. In the process of clean reaction and short processing time modification, the surface of the material is endowed with desirable and ideal physical and chemical properties without negatively affecting the bulk structure [20].

Low temperature plasma, an effective surface modification method, has been used for the surface pre-treatment of sulfide minerals to increase the separation efficiency between minerals. Excellent separation efficiency was achieved by the treatments of pyrite, chalcopyrite, molybdenite and chalcocite in Ar/O<sub>2</sub> microwave (MW) and radio frequency (RF) discharges [21–24]. The results showed a significant difference in the surface oxidation rates of various sulfides in low temperature plasma [21,22]. The oxidation rate of chalcopyrite is 8.4 and 19.1 times faster than that of pyrite and chalcocite, respectively [21]. Pyrite in mixed minerals delayed the emission of sulfur dioxide (SO<sub>2</sub>) from the oxidation of mineral Cu<sub>2</sub>S in low temperature plasma, which resulted from the different oxidation rates of pyrite and chalcocite [22]. The original sulfide/sulfide of sulfide mixtures was converted into oxide/sulfide system, proving that the selective surface modifications of mineral mixtures by low temperature plasma pre-treatment are feasible [24]. However, none of the retrieved literature considered the effects of low temperature oxygen plasma modification on the floatability of arsenopyrite and the separation efficiency of pyrite from arsenopyrite.

In this study, surface modification with dielectric barrier discharge (DBD) low temperature oxygen plasma was performed to increase the separation efficiency of pyrite and arsenopyrite. The effects of plasma modification on the arsenopyrite and pyrite surface were assessed by micro-flotation tests, X-ray photoelectron spectroscopy (XPS) studies, Fourier transform infrared spectroscopy (FTIR) analysis, inductively coupled plasma mass spectrometry (ICP-MS) analysis and zeta potential measurements.

## 2. Materials and Methods

### 2.1. Experimental Setup

The schematic view of the setup applied in the experiments is shown in Figure 1. The power supply was provided by Nanjing Surman Plasma Technology Co. Ltd. (Nanjing, China). The DBD reactor was a self-made quartz tube with a height of 260 mm, an external diameter of 21 mm and an internal diameter of 19 mm. The HV electrode was a stainless-steel bar with a diameter of 2 mm,

arranged in the center of the reactor. A layer of tin foil was wrapped around the reactor as the LV electrode. Before the plasma pre-treatment experiment, gas-permeable quartz sand was arranged in the middle of the reactor and the sample was transferred onto the quartz sand.

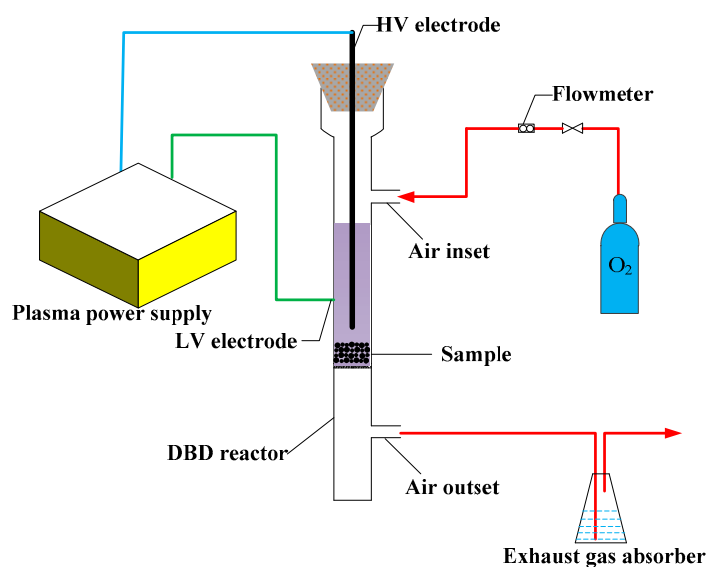


**Figure 1.** Schematic view of the plasma recipient.

## 2.2. Materials and Reagents

The representative pyrite and arsenopyrite samples employed in all the experiments were obtained from Yunnan province, China. For micro-flotation experiments and XPS analysis, the pyrite and arsenopyrite samples were overall crushed with an agate mortar. Subsequently, the fine-grained pyrite and arsenopyrite particles were sieved using Tyler screens to achieve a particle fraction of  $-105 + 38 \mu\text{m}$ . Besides, the fractions finer than  $10 \mu\text{m}$  were screened for FTIR spectroscopic analysis and zeta potential measurements. Furthermore, the whole fractions finer than  $105 \mu\text{m}$  for ICP-MS analysis. The chemical analysis suggested that the pyrite samples contained 45.87% Fe and 53.39% S and the arsenopyrite samples contained 34.30% Fe, 45.18% As and 19.69% S, which indicated that purity of pyrite and arsenopyrite samples were overall higher than 95%. To prevent the mineral surface from the oxidation, the samples employed in all experiments were ultrasonically cleaned and then vacuum dried.

Sodium butyl xanthate (SBX) served as the collector. The pH values of the solution were regulated using 0.1 mol/L sodium hydroxide (NaOH) and 0.1 mol/L hydrochloric acid (HCl) solutions. All reagents employed in this study were of analytical grade and deionized water was used throughout the experiments.

## 2.3. Sample Pre-treatment

For each experiment, 7 g of ultrasonically cleaned and vacuum dried ore sample was transferred to the reactor and placed uniformly on quartz sand. Subsequently, the piston with a HV electrode was plugged into the reactor and the lower end of the HV electrode was positioned 5 mm above the ore sample. Pre-inflate for half a minute before plasma ignition to remove residual air from the reactor. In the meantime, the flow rate of oxygen was controlled by the mass flow meter to 210 mL/min. Next, the voltage regulator was rotated to the required input voltage (30 V, 35 V, 40 V, 45 V) and the input current was adjusted to  $1.2 \pm 0.1 \text{ A}$ . The timing started after the current was stable and the pre-treatment time was 30 s, 1 min, 2 min, 3 min, 4 min and 5 min, respectively.

A temperature probe (Testo108, GER) was used to measure the temperatures during the plasma modification. The highest temperatures at input voltages of 30 V, 35 V, 40 V and 45 V were 328.5 K,

333.4 K, 342.1 K and 355.4 K, respectively. The DBD reactor containing 7.0 g samples was placed in the above constant temperatures water and keep the liquid level above the sample position and inflating for 1 min at the oxygen flow rate of 210 mL/min. The same flotation procedure was used to investigate the effect of temperature on the separation efficiency of arsenopyrite and pyrite.

#### 2.4. Flotation Experiments

The sample used in the flotation experiments was a mixed sample of arsenopyrite and pyrite with a mixed ratio of 1:1 by weight. Flotation experiments were performed in a 40-mL XFG flotation cell with an impeller speed of 1500 rpm and 5.0 g mixed samples were placed in 40 mL deionized water.  $1 \times 10^{-4}$  mol/L SBX solution was poured into the suspension and agitated for 3 min. The flotation was performed for 5 min. Native pH (about 6.5) and no depressants or frothers were employed for the flotation experiments. The concentrates and tailings were overall weighed to calculate the flotation recovery and separation efficiency. Each flotation experiment was measured three times.

#### 2.5. XPS Measurements

XPS measurements were performed using a Thermo Scientific apparatus (250 Xi, Thermo fisher Scientific, Waltham, MA, USA) with an Al  $K_{\alpha}$  X-ray source. To determine all elements in the measured sample, a survey scan was first performed at pass energy of 100 eV. Subsequently, multiplex (narrow) high resolution scan was performed at 30 eV to obtain the XPS spectrum of each specific element. The Thermo Avantage software was employed for data processing and fitting. The spectral intensities were converted to surface elemental concentrations by initially subtracting a Shirley-type background and then fitting peaks using an 80% to 20% Gaussian/Lorentzian line shape. The binding energies were calibrated using C 1s spectrum photoelectron peak (adventitious carbon, C-C) as a reference with a binding energy of 284.8 eV.

#### 2.6. FTIR Spectroscopic Analysis

The infrared spectra of the untreated and plasma-modified samples were recorded with a Nicolet iS 10 Fourier Transform Infrared Spectrometer (Thermo fisher Scientific, Waltham, MA, USA) by KBr diffuse reflection method. The scanned area was from 4000 to 400  $\text{cm}^{-1}$ . Each spectrum was recorded with 16 scans measured at 4  $\text{cm}^{-1}$  resolution.

#### 2.7. Zeta Potential Measurements

The zeta potentials of the arsenopyrite and pyrite before and after plasma pre-treatment were performed using a Brookhaven ZetaPlus zeta potential analyzer (Brookhaven, NY, USA). By mixing 0.1 g sample with 40 mL of deionized water containing  $5 \times 10^{-3}$  mol/L  $\text{KNO}_3$  background solutions, the mineral suspension was prepared. For each experiment, the suspension pH was adjusted to a desired value using 0.1 mol/L HCl or 0.1 mol/L NaOH stock solutions. If necessary,  $1 \times 10^{-4}$  mol/L freshly prepared SBX solution was added into the suspension before pH adjustment. The prepared suspension was magnetically stirred for 5 min by a magnetic stirring apparatus. The resultant suspensions were allowed to stand still for 10 min and the supernatant of the suspension was transferred to a measuring vessel using a plastic dropper for zeta potential measurements at ambient temperature. The  $\zeta$  potential of each sample was measured three times [25].

#### 2.8. Dissolution of Arsenopyrite and Pyrite by ICP Analysis

The concentrations of Fe and S (pyrite and arsenopyrite) and As (arsenopyrite) dissolved in arsenopyrite and pyrite before and after low temperature oxygen plasma were measured by ICP-MS (ELAN-DRC II, PE, MA, USA). The suspension was prepared by adding 2 g sample into the 100 mL deionized water and subsequently the prepared suspension was stirred by a magnetic stirring apparatus for a certain time. The supernatant was aspirated by a Pasteur pipette and transferred to two

15 mL centrifugal tubes, centrifuged at a speed of 3000 r/min for 30 min by a centrifuge. Then 10 mL of supernatant was obtained as ICP-MS measurement sample. The concentration of each element was measured three times.

### 3. Experimental Results

#### 3.1. Flotation Experiments Results

The flotation performances of the arsenopyrite and pyrite as a function of low temperature oxygen plasma pre-treatment time were evaluated and the results are shown in Figure 2. The concept of separation efficiency was adopted to calculate the difference of the recovery by the same plasma pre-treatment time between pyrite and arsenopyrite, which is calculated by Equation (1) [26]:

$$SE = R(\text{pyrite}) - R(\text{arsenopyrite}) \quad (1)$$

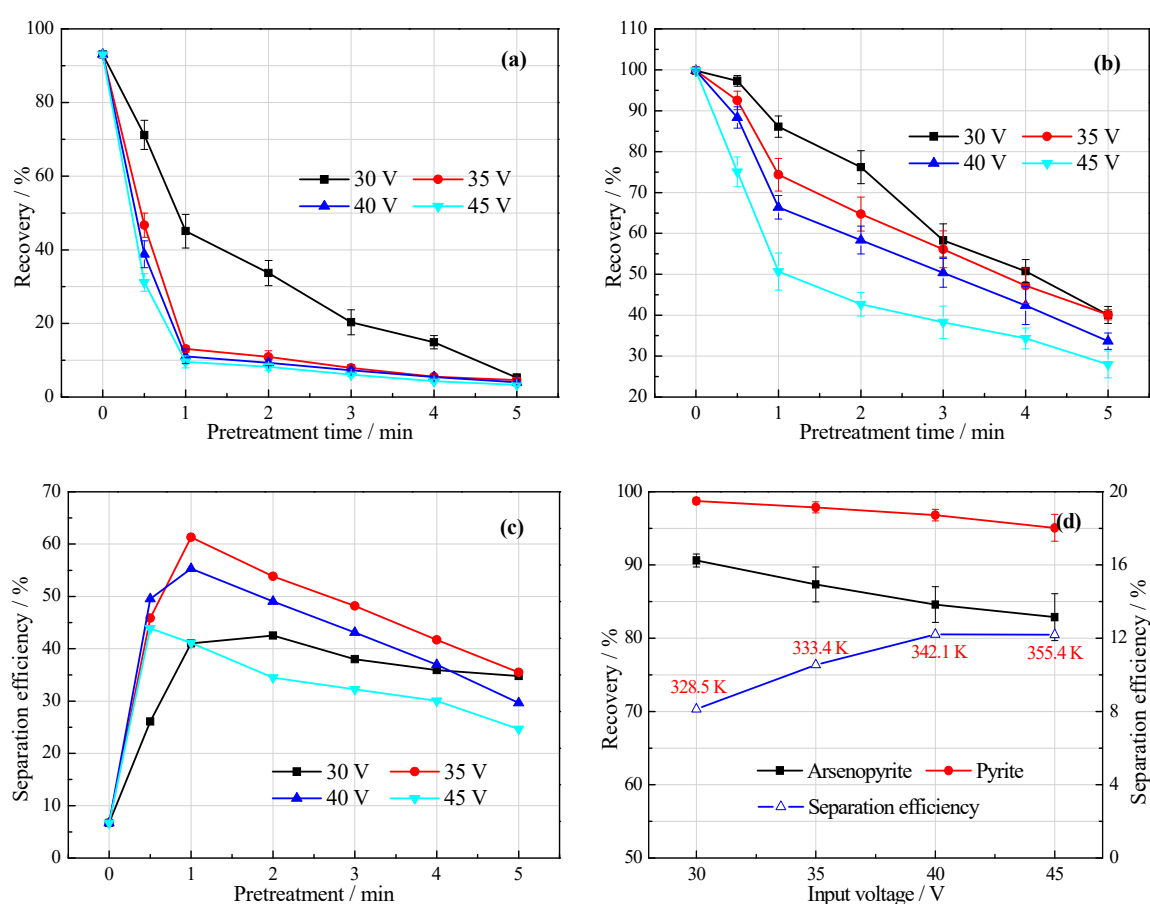


**Figure 2.** Relationship between of flotation recovery of arsenopyrite (a) and pyrite (b) and separation efficiency (c) and pre-treatment time and temperature (d) in native pH with  $1 \times 10^{-4}$  M SBX as a collector.

Figure 2 indicates that without plasma pre-treatment, the recoveries of arsenopyrite and pyrite reached 93.12% and 99.81%, respectively. A paired *t*-test was used to determine whether there was any significant difference in the flotation recovery before and after plasma modification. The results of the *t*-test (Table A1) indicate that, regardless of the input voltage, the mean differences between the pyrite recovery and arsenopyrite recovery after plasma modified were significantly changed based on *p*-values (both of *p*-values were less than 0.05). It can be seen from Figure 2d that the modification temperature has an effect on the flotation recovery of arsenopyrite and pyrite. With the increase in

modification temperature, the recovery of arsenopyrite and pyrite decreases gradually, while the separation efficiency presents an increasing tendency. However, although the *p*-values were less than 0.05 (Table A2), the mean recoveries of arsenopyrite and pyrite were all greater than 80% (Figure 2d) at the plasma-modification temperature in this study. The flotation recovery of both samples decreased gradually with the extension of the plasma pre-treatment. Elevated voltage accelerated the reduction of the floatability of arsenopyrite and pyrite. However, excessive input voltage will increase the hydrophilicity of pyrite, thereby reducing the flotation separation efficiency. The flotation recovery of arsenopyrite decreases sharply at a shorter pre-treatment time (1 min), while pyrite remains relatively high floatability. A longer treatment time of plasma does not result in significant changes in the recovery of arsenopyrite, while the recovery of pyrite is still reduced. Therefore, in this study, the separation efficiency is the highest at a shorter treatment time (1 min) and lower input voltage (35 V), which is considered the optimal separation condition of arsenopyrite and pyrite (Figure 2c).

### 3.2. XPS Analysis Results of Arsenopyrite

XPS analysis can show the chemical properties of material surface. The chemical composition and states of the surfaces of the plasma-modified and bare arsenopyrite were distinguished by XPS based on the unique binding energy of various elements [27]. The atomic concentrations and relative species distributions of a specific element on the surfaces of untreated and plasma-treated arsenopyrite were calculated and fitted with the Thermo Avantage software. The XPS narrow spectra of Fe2p, As3d, S2p and O1s of the arsenopyrite samples are shown in Figure 3 and the fitting results of atomic concentrations and relative species distributions are listed in Table 1.

**Table 1.** Iron, arsenic, sulphur and oxygen peak parameters, proportions and chemical states/bonding of arsenopyrite before and after treated by low temperature oxygen plasma.

Spectral Peak	Binding Energy (eV)		Species Distribution (%)		Atomic Concentration (%)		Chemical State
	Untreated	Plasma-Treated	Untreated	Plasma-Treated	Untreated	Plasma-Treated	
Fe(2p <sub>3/2</sub> )	706.1	706.1					Fe(II)-(AsS)
Fe(2p <sub>3/2</sub> )	707.1	707.1	61.2	57.3			
Fe(2p <sub>3/2</sub> )	708.1	708.1					
Fe(2p <sub>3/2</sub> )	709.4	709.4			9.0	7.9	Fe(III)-(AsS)
Fe(2p <sub>3/2</sub> )	710.6	710.6	28.5	31.2			
Fe(2p <sub>3/2</sub> )	711.6	711.6					
Fe(2p <sub>3/2</sub> )	712.4	712.4			10.3	11.5	Fe(III)-O
Fe(2p <sub>3/2</sub> )	713.4	713.4					
Fe(2p <sub>3/2</sub> )	714.4	714.4					
As(3d <sub>5/2</sub> ) <sup>1</sup>	41.3	41.2	52.8	52.9	29.5	27.5	As(-I)-S
As(3d <sub>5/2</sub> ) <sup>1</sup>	41.8	41.8	8.9	5.8			As(0)
As(3d <sub>5/2</sub> ) <sup>1</sup>	43.4	43.4	12.7	14.3			As(I)-O
As(3d <sub>5/2</sub> ) <sup>1</sup>	44.3	44.3	12.3	14.0			As(III)-O
As(3d <sub>5/2</sub> ) <sup>1</sup>	45.4	45.3	13.3	13.0			As(V)-O
S(2p <sub>3/2</sub> ) <sup>2</sup>	161.3	161.3	13.7	11.3	23.9	21.9	S <sup>2-</sup>
S(2p <sub>3/2</sub> ) <sup>2</sup>	162.3	162.2	57.9	55.0			S <sub>2</sub> <sup>2-</sup>
S(2p <sub>3/2</sub> ) <sup>2</sup>	163.4	163.4	17.2	17.2			S <sub>n</sub> <sup>2-</sup>
S(2p <sub>3/2</sub> ) <sup>2</sup>	166.4	166.4	7.3	6.1			S <sub>2</sub> O <sub>3</sub> <sup>2-</sup>
S(2p <sub>3/2</sub> ) <sup>2</sup>	168.4	168.4	3.9	10.4			SO <sub>4</sub> <sup>2-</sup>
O(1s)	530.7	530.6	52.3	43.1	37.6	42.7	Fe-O
O(1s)	531.6	531.5	38.1	48.6			As-O
O(1s)	533.2	533.0	9.6	8.3			S-O

<sup>1</sup> This peak has a doublet fitted at 0.7 eV higher binding energy with the same FWHM value and two-thirds of the area of the peak listed. The doubles have been employed to fit the As3d spectra of Figure 3 but not included in the table. <sup>2</sup> This peak has a doublet fitted at 1.2 eV higher binding energy with the same FWHM value and one-half of the area of the peak listed. The doubles have been employed to fit the S2p spectra of Figure 3 but are included in the table.

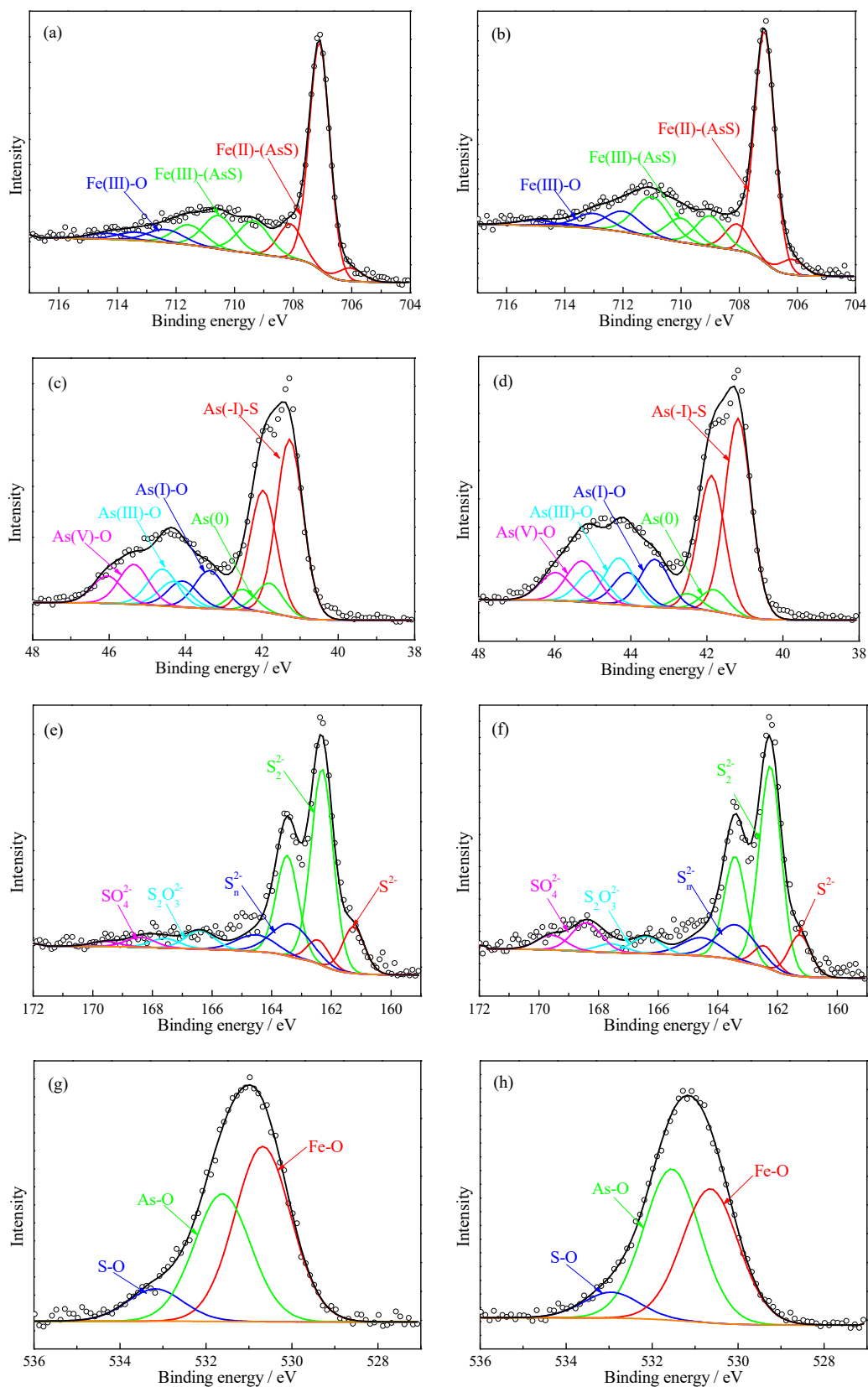


**Figure 3.** X-ray photoelectron spectroscopy (XPS) Fe2p (a), As3d (c), S2p (e), O1s (g) spectra of arsenopyrite and Fe2p (b), As3d (d), S2p (f), O1s (h) spectra of arsenopyrite after treated by low temperature oxygen plasma for 1 min at 35 V (the circles represent the XPS data and the thick curves represent the fitted data).

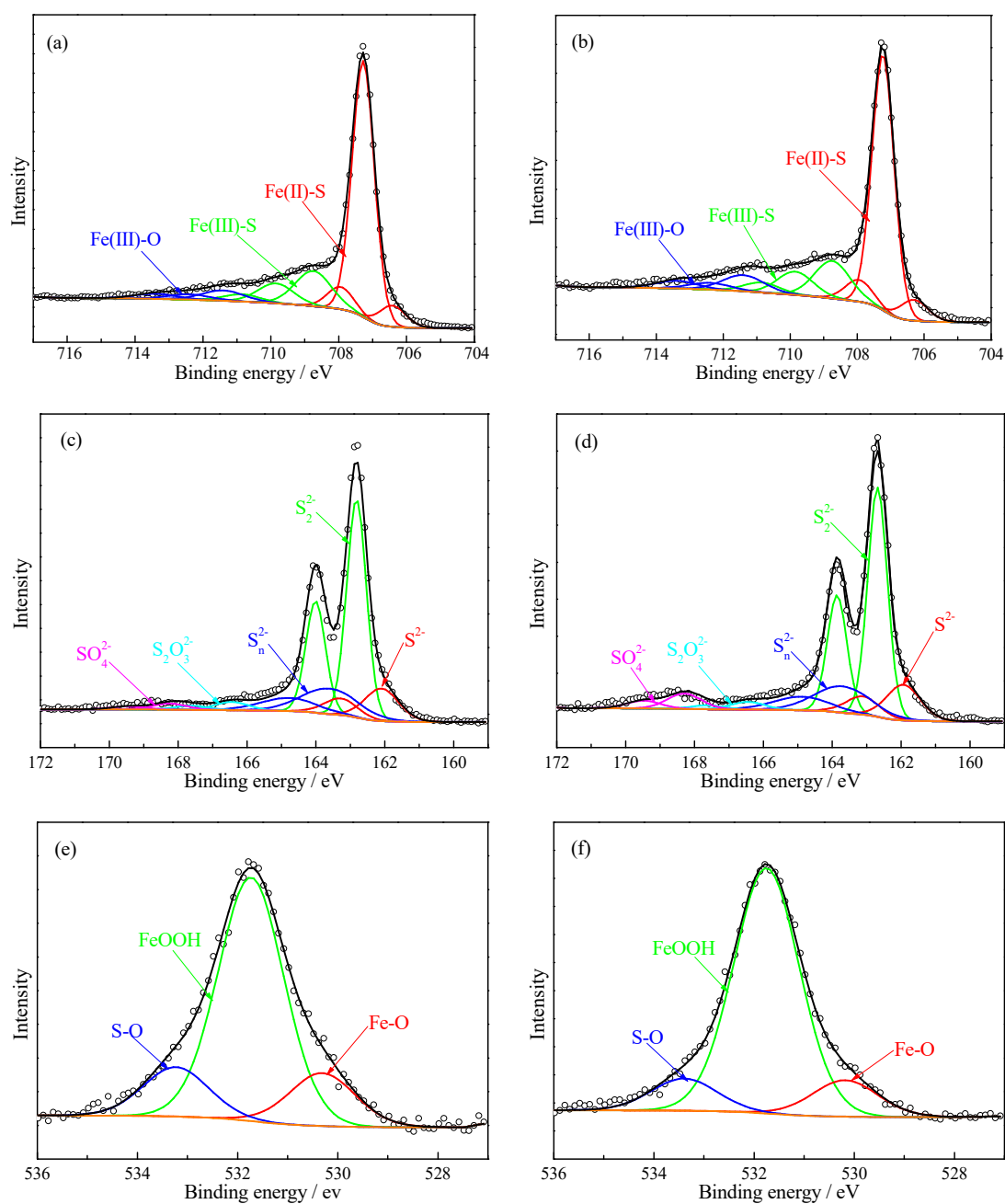
For the Fe2p spectrum, based on the theoretical core *p* level multiplet structures (GS multiplets) for free transition elements, Fe(II) has three major multiplet peaks and Fe(III) yields three major multiplet peaks at relative lower binding energy (709.4–711.6 eV) [28]. To accurately compare the changes in the relative species distributions of arsenopyrite before and after the plasma treated, an equal full width half maximum peak width (FWHM) was arranged at the same binding energy. The Fe2p XPS spectra at lower binding energy side (706.1–708.1 eV) can be attributed to Fe(II)-(AsS) [29]. Since the Fe(II) bonded to As-As, As-S or S-S is essentially the same in bonded energy, the Fe(II)-(AsS) peak in this study represents the sum of Fe(II)-(AsS) and Fe(II)-(S<sub>2</sub>) [28,29]. The higher binding energy side (712.4–714.4 eV) corresponded to Fe(III)-O formed on the arsenopyrite surface with three multiplet peaks [29,30]. After plasma modified, the atomic concentration of Fe on the surface of arsenopyrite was decreased from 9.0% to 7.9%, while the content of O was increased from 37.6% to 42.7%. In addition, compared with the bare samples, the proportions of Fe(III)-(AsS) and Fe(III)-O after plasma modified increased from 28.5% and 10.3% to 31.2% and 11.5%, respectively, while the content of Fe(II)-(AsS) was significantly reduced from 61.2% to 57.3%.

Figure 3 shows the As3d spectrum of untreated (c) and plasma-treated (d) arsenopyrite. The As3d spectrum of arsenopyrite were fitted by five pairs split peaks. The optimal fitting for arsenopyrite yielded a major peak at 41.3 eV accounting, interpreted as As(-I)-S, while a small peak at 41.8 eV was attributed to As(0) [29,31]. The high binding energy of As3d spectrum indicates the presence of As in higher oxidation states. Three additional peaks at 43.4, 44.3 and 45.4 eV represent the species of As(I)-O, As(III)-O and As(V)-O, respectively [29]. In comparison with the bare samples, the total amount of As on the plasma-modified arsenopyrite surface decreased from 29.5% to 27.5%. However, the contents of high oxidation states of As (III) and As (V) did not increase after the pre-treatment by plasma, while more changes occurred in the oxidization of As(-I)-S and As(0) to lower oxidized state of As(I)-O.

The S2p<sub>3/2</sub> spectrum of arsenopyrite was fitted with six spin-orbit doublet peaks (Figure 3e,f). The first doublet of the S2p<sub>3/2</sub> level with binding energy of 161.3 eV corresponded to S in monosulfides formed on the surfaces of arsenopyrite [29,31]. The second and third doublets formed at binding energies of 162.3 eV and 163.4 eV were attributed to disulfide and polysulfide [29]. The higher binding energies at 166.4 eV and 168.4 eV were attributed thiosulfate and sulfate, respectively [29,32]. The atomic concentration of S on the arsenopyrite surface decreased from 23.9% to 21.9% after the modification of low temperature oxygen plasma and the proportion of monosulfide and disulfide favorable for the arsenopyrite flotation fell from 13.7% and 57.9% to 11.3% and 55.0%, respectively. Furthermore, the surface component of sulfate increased significantly from 3.9% to 10.4% on the plasma-pre-treatment arsenopyrite surface.

### 3.3. XPS Analysis Results of Pyrite

The XPS narrow spectra of Fe2p, S2p and O1s of the pyrite samples shown in Figure 4 and the results of fitted peak parameters including atomic concentration, binding energy and relative species distribution are listed in Table 2. The detailed assignments of S, Fe and O were determined according to the references and summarized in Table 1 [33]. After plasma modified, the content of O on the pyrite surface increased from 21.5% to 29.8% and the atomic concentration of Fe and S decreased from 14.0% and 64.5% to 12.9% and 57.3%, respectively. In addition, the reduction of S atomic concentration (7.2%) of plasma-pre-treatment pyrite was more significantly than that of Fe (1.1%). In other words, the ratio of S/Fe on the surface of bare pyrite (4.6) was greater than the plasma-modification samples (4.4).



**Figure 4.** XPS Fe2p (a), S2p (c), O1s (e) spectra of pyrite and Fe2p (b), S2p (d), O1s (f) spectra of pyrite after treated by low temperature oxygen plasma for 1 min at 35 V (the circles represent the XPS data and the thick curves represent the fitted data).

The same GS multiplets method used for fitting the arsenopyrite was employed to analyze the Fe2p<sub>3/2</sub> XPS spectra of pyrite before and after plasma treated. According to Table 2, the Fe2p<sub>3/2</sub> XPS spectra of plasma-modified pyrite show similar fitting results with arsenopyrite (Table 1). Compared with the bare pyrite, the concentration of Fe(II)-S decreased by 4.5% on the plasma-modified pyrite surface, while the proportions of Fe(III)-S and Fe(III)-O increased by 1.2% and 3.3%, respectively. Moreover, the proportion of sulfate increased from 2.9% to 6.6% after low temperature oxygen plasma modification.

**Table 2.** Iron, sulphur and oxygen peak parameters, proportions and chemical states/bonding of pyrite before and after treated by low temperature oxygen plasma.

Spectral Peak	Binding Energy (eV)		Species Distribution (%)		Atomic Concentration (%)		Chemical State
	Untreated	Plasma-Treated	Untreated	Plasma-Treated	Untreated	Plasma-Treated	
Fe(2p <sub>3/2</sub> )	706.4	706.3					
Fe(2p <sub>3/2</sub> )	707.3	707.2	68.7	64.2			Fe(II)-S
Fe(2p <sub>3/2</sub> )	708.0	708.0					
Fe(2p <sub>3/2</sub> )	708.8	708.8			14.0	12.9	
Fe(2p <sub>3/2</sub> )	709.9	709.9	22.7	23.9			Fe(III)-S
Fe(2p <sub>3/2</sub> )	710.9	710.9					
Fe(2p <sub>3/2</sub> )	711.4	711.4					
Fe(2p <sub>3/2</sub> )	712.4	712.4	8.6	11.9			Fe(III)-O
Fe(2p <sub>3/2</sub> )	713.4	713.4					
S(2p <sub>3/2</sub> ) <sup>1</sup>	162.1	161.9	15.0	15.1			S <sup>2-</sup>
S(2p <sub>3/2</sub> ) <sup>1</sup>	162.8	162.7	58.7	56.5			S <sub>2</sub> <sup>2-</sup>
S(2p <sub>3/2</sub> ) <sup>1</sup>	163.6	163.7	19.6	18.6	64.5	57.3	S <sub>n</sub> <sup>2-</sup>
S(2p <sub>3/2</sub> ) <sup>1</sup>	166.5	166.5	3.8	3.2			S <sub>2</sub> O <sub>3</sub> <sup>2-</sup>
S(2p <sub>3/2</sub> ) <sup>1</sup>	168.3	168.3	2.9	6.6			SO <sub>4</sub> <sup>2-</sup>
O(1s)	530.3	530.2	15.3	11.6			Fe-O
O(1s)	531.7	531.8	70.4	78.1	21.5	29.8	FeOOH
O(1s)	533.2	533.4	14.3	10.3			S-O

<sup>1</sup> This peak has a doublet fitted at 1.2 eV higher binding energy with the same FWHM value and one-half of the area of the peak listed. The doubles have been used to fit the S2p spectra of Figure 4 but are not included in the table.

### 3.4. FTIR Spectroscopic Analysis Results

FTIR reflection spectra of SBX adsorption on the bare and plasma-modified arsenopyrite and pyrite with the SBX concentration of  $1 \times 10^{-4}$  M is shown in Figure 5. The characteristic absorption bands of dixanthogen at about  $1261.22 \text{ cm}^{-1}$  and  $1031.91 \text{ cm}^{-1}$  are observed when bare arsenopyrite is conditioned in SBX solution [34]. However, characteristic band at  $1261.22 \text{ cm}^{-1}$  on the plasma-modified arsenopyrite disappeared. In contrast, the characteristic adsorption bands on the surface of pyrite does not show significantly changes, whether or not was modified by plasma.

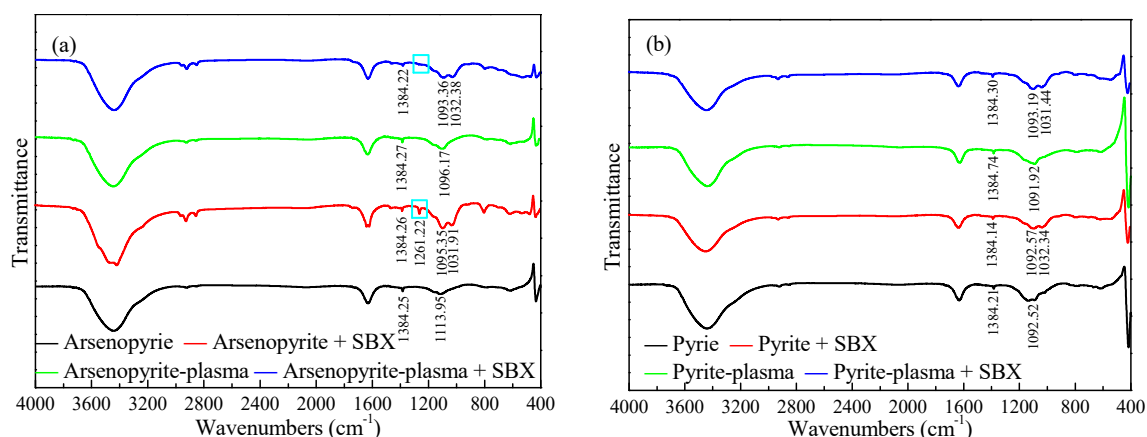


**Figure 5.** Fourier transform infrared (FTIR) spectra of arsenopyrite (a) and pyrite (b) before and after plasma-modified with  $1 \times 10^{-4}$  M SBX as the collector (pre-treatment time 1 min, input voltage 35 V).

### 3.5. ICP-MS Analysis Results

When the arsenopyrite and pyrite particles contact with water in the flotation pulp, some components (e.g., Fe, As and S) on the surfaces of minerals transfer to the liquid phase in an ionic state (e.g.,  $\text{Fe}^{2+}$ ,  $\text{Fe}^{3+}$ , As(I), As(III), As(V),  $\text{SO}_4^{2-}$  and  $\text{S}_2\text{O}_3^{2-}$ , etc.), which changes the distributions and states of elements on the mineral surfaces and then affecting the surface properties and their flotation behavior. The oxidation of sulfide minerals is closely related to the solubility and oxidation facilitates the dissolution of sulfide minerals, especially heavy metal ions [35]. The effects of plasma

pre-treatment on dissolution of arsenopyrite and pyrite surface are shown in Figure 6. In all the experiments, the output concentration of each component dissolved in aqueous solution increased with the extension of stirring. There was a statistical evidence (both of  $P$ -values were less than 0.05) that the plasma modification enhanced the dissolution of Fe and S from the arsenopyrite and pyrite samples in aqueous solution within 5 h leaching time (Tables A3 and A4). In contrast, the  $t$ -test showed that there was no statistically significant difference (both of  $p$ -values were greater than 0.05) in the arsenic concentrations released from the plasma-modification arsenopyrite and the bare arsenopyrite (Table A3).

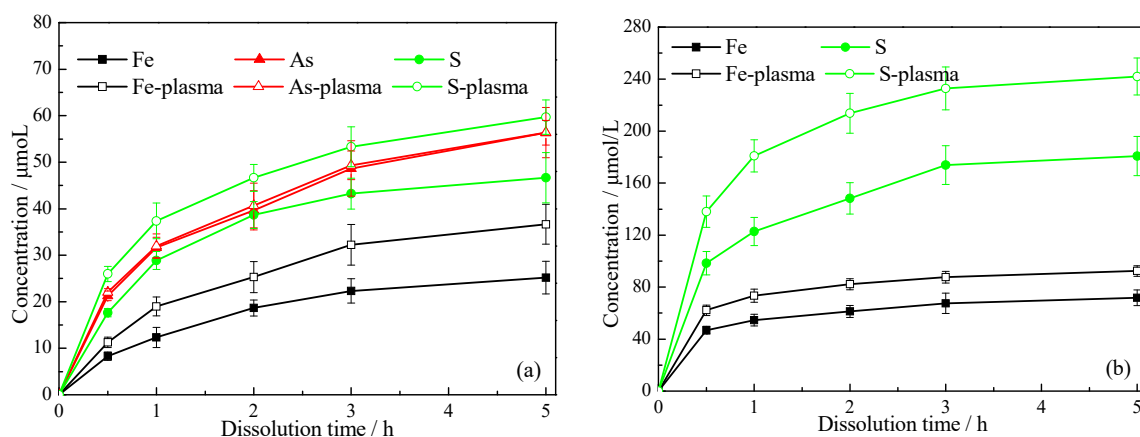


**Figure 6.** Ions concentrations released from the arsenopyrite (a) and pyrite (b) at natural pH with and without plasma modified (pre-treatment time 1 min, input voltage 35 V).

### 3.6. Zeta Potential Determination Results

Zeta potential is an effective means for determining the interaction of mineral surfaces with flotation reagents in the flotation process [36,37]. In this study, the plasma surface modification of arsenopyrite and pyrite has been investigated by measuring zeta potentials of minerals with a wide pH range. Figure 7 shows that the zeta potentials of bare arsenopyrite and pyrite particles decreased with the increase of solution pH. The isoelectric point (IEP) of bare arsenopyrite and pyrite without the addition of collectors were achieved at pH 0.6 and 2.7, respectively. Plasma modification greatly contributed to the positive shifts of zeta potential values of arsenopyrite and pyrite and the IEP shifted to the higher pH 2.14 and 3.22 after plasma modification. In addition, there was no statistically significant difference (both the  $p$ -values were greater than 0.05) in the zeta potentials of the bare arsenopyrite in the presence and absence of SBX in the pulp with pH greater than 9 (Table A5). Likewise, there was no statistically significant difference (both the  $p$ -values were greater than 0.05) in the zeta potentials of the bare arsenopyrite in the presence and absence of SBX in the pulp with pH greater than 5 (Table A5). However, there was a statistical evidence (both the  $p$ -values were less than 0.05) that the zeta potentials of the plasma-modification pyrite in the presence of SBX were less than that in the absence of SBX within a wide pH range ( $\text{pH} \leq 9$ ) (Table A6).

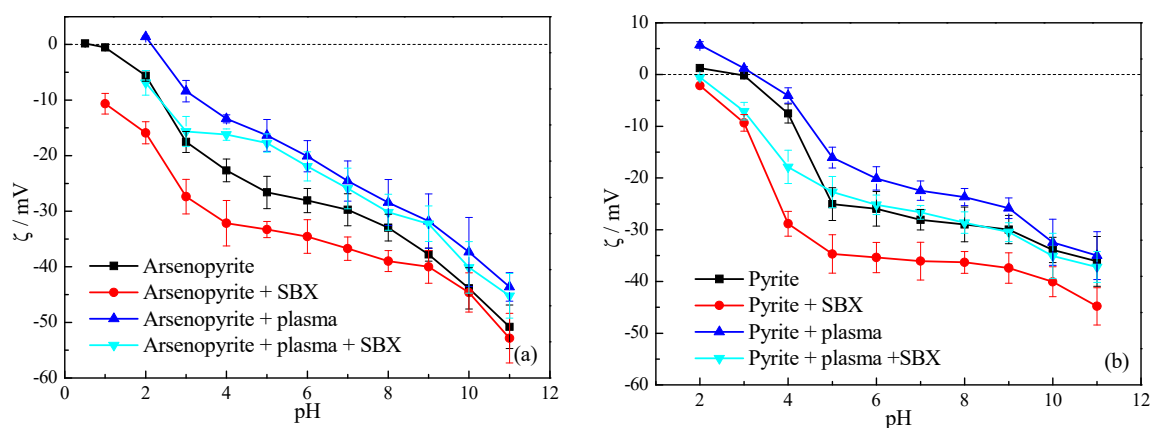


**Figure 7.** Zeta potentials of arsenopyrite (a) and pyrite (b) as a function of pH before and after plasma modified with  $1 \times 10^{-4}$  M sodium butyl xanthate (SBX) as the collector (pre-treatment time 1 min, input voltage 35 V).

#### 4. Discussion

This study showed that the low temperature oxygen plasma can achieve effective separation of minerals. The effects of plasma on the floatability of arsenopyrite are stronger than that of pyrite, which is consistent with the fact that arsenopyrite is more sensitive to oxidation than pyrite [38]. The pre-treatment time of the oxygen plasma had a negative correlation with the flotation recovery. The reactions of excitation, dissociation and ionization of oxygen took place at the plasma ignition, through which the reactive species were produced [39]. With the increase in plasma pre-treatment time, more reactive species have the opportunity to bombard the mineral surfaces, thereby breaking the original covalent bonds of the crystals and promoting the oxidation and increasing the hydrophilic of mineral surfaces by binding O with Fe-, As- and S- [40].

With a constant input current ( $1.2 \pm 0.1$  A), a higher input voltage indicates higher input power and output power in the experiment system. It is generally believed that the reaction rate increased at high input power is correlated with the energy density. Accordingly, the acceleration in reaction rates can be interpreted by higher densities of reactive oxygen species as well as by rising the gas temperatures [21]. In other words, higher input voltage has higher density of reactive species and reaction temperature. The modification temperature experiments (35 V, 1 min) indicated that the recovery of arsenopyrite and pyrite decreased to 88.35% and 97.51%, respectively. Though the modification temperature increased the separation efficiency of pyrite from arsenopyrite to a certain extent, the changes of minerals hydrophobicity should be primarily attributed to the reaction of the plasma reactive species with the mineral surfaces. It is noteworthy that excessive input voltage will increase the hydrophilicity of pyrite, thereby reducing the flotation separation efficiency.

This study indicates that the effects of plasma modification on the surface properties of arsenopyrite and pyrite are attributed to the changes of the concentrations of oxidation products. XPS analysis indicates that low temperature oxygen plasma pre-treatment of the arsenopyrite surface resulted in substantial enrichment of O and diminution of Fe, As and S. Under the modification of the plasma reaction species, the original sulfide on the surface of arsenopyrite was converted into sulfide/oxide mixed. Consistent with arsenopyrite, oxygen-enrichment region was formed on the surface of low temperature oxygen plasma-modified pyrite. However, the O atomic concentrations on the untreated (21.5%) or plasma-modified (29.8%) pyrite surfaces were much lower than that of the arsenopyrite (37.6% and 42.7% respectively), which may be one of the reasons for the difference of hydrophobicity between the arsenopyrite and pyrite.

In addition, compared with the samples of untreated, the proportions of Fe(III)-O and  $\text{SO}_4^{2-}$  on the surfaces of plasma-modified arsenopyrite and pyrite increased, while the concentrations of iron sulfides, monosulfide and polysulfide favorable for flotation show a decreasing tendency. After plasma

pretreated, the original sulfide states of the elements Fe and S were oxidized to a more hydrophilic oxidation state. Moreover, the changes of chemical states proportions enhanced the dissolutions of the mineral particles. The lack of iron sulfides and dissolution of iron ions on the surfaces of the plasma-modified minerals resulted in a lower reaction opportunity between the mineral surfaces and collector, which decreased the flotation recovery. It is also noteworthy that the proportions of hydrophilic sulfates and iron oxides species on the pyrite surfaces after plasma pretreated were significantly lower than those of arsenopyrite, which may be another reason for the difference in hydrophobicity between the arsenopyrite and pyrite.

In particular, the proportion of high oxidation states of arsenic on the surface of plasma-modified arsenopyrite was not significantly changed, which is probably correlated with arsenic was the most readily oxidized element in the arsenopyrite surfaces [41]. Consistent with the slight changes in the concentrations of high-valence As(III)-O and As(V)-O (Table 1), plasma has little effect on the dissolution of arsenic on the arsenopyrite surface. In addition, the concentrations of arsenic and sulfur dissolved from arsenopyrite surface were higher than those of iron, suggesting that the measured elemental ratios in the solution are different from those in the solid phase of arsenopyrite. A similar phenomenon was also observed in the dissolution experiments of pyrite. The non-equimolar ion concentrations indicated that the dissolution of the oxidized arsenopyrite and pyrite is proceeded non-stoichiometrically, which is primarily correlated with the degree of oxidation of mineral components [42]. Plasma modification further increased the differences of “incongruently” or “non-stoichiometrically” dissolution of the mineral components and resulted in a significantly increase in the S/Fe ration of the mineral surfaces. Since the interaction sites on the arsenopyrite and pyrite surfaces with flotation reagents are iron, the decrease in Fe concentration on the mineral surfaces has negative effects on flotation recovery [30].

In the presence of SBX, the zeta potentials of arsenopyrite and pyrite surfaces became further negative. This indicates that the negatively charged collector adsorbed on the mineral surfaces. With the pH range tested here, most of the zeta potentials of the sample surfaces were negative, suggesting that a chemical adsorption took place through the interaction between collector and the negatively charged arsenopyrite and pyrite surfaces [27]. Regardless of the bare or the plasma-modified arsenopyrite particles, the extent of negative zeta potential change on the mineral surfaces was increased with the increase in the pulp pH. In the pulp with pH greater than 9, a slight effect of SBX on the zeta potentials of the bare arsenopyrite surface was observed from Figure 6a, indicating that there was low adsorption concentration of xanthate on the surface of the arsenopyrite in the alkaline pulp solution (pH > 9). Flotation of arsenopyrite in the pulp using SBX as the collector has been attributed to the oxidation reaction of the xanthate ions ( $X^-$ ) to dixanthogen ( $X_2$ ), which can be described as follows [3]:



The mentioned change in the zeta potential can be primarily attributed to the pulp redox potential ( $E_H$ ) values in the alkaline pulp solution below the reversible potential for the  $X^-/X_2$  pair [3]. A similar trend was found on the plasma-modified arsenopyrite when the pulp pH was larger than 5, suggesting that the plasma pre-treatment reduced the formation of dixanthogen on the mineral surface. Consistent results were obtained from the results of FTIR spectroscopic analysis, the disappearance of characteristic band of dixanthogen at  $1261.22\text{ cm}^{-1}$  on the plasma-modified arsenopyrite. As a result, the adsorption of xanthate on the surface of the arsenopyrite only occurred in strongly acidic pulp solution. Compared with arsenopyrite, plasma had slight effects on the adsorption of SBX on the surface of pyrite. The differences in the adsorption of xanthate on the mineral surfaces lay the conditions for flotation separation of pyrite from arsenopyrite by low temperature oxygen plasma modified.

## 5. Conclusions

To evaluate the underlying mechanisms of the mineral surface modification process and selective flotation, detailed surface analysis was investigated for plasma modified arsenopyrite and pyrite. On the basis of the above discussion and results, the major conclusions were summarized as follows:

Low-temperature oxygen plasma can achieve selective modification of the surface of arsenopyrite and pyrite by controlling the reasonable treating time and input voltage. The modified arsenopyrite was completely hydrophilic, while pyrite still showed an excellent flotation performance.

XPS analysis indicated that the oxidation degree of arsenopyrite was much higher than that of pyrite. Plasma modification resulted in the formation of arsenopyrite surface of substantial enrichment of O and diminution of Fe, As and S. A large number of iron and sulfur on the plasma-modification arsenopyrite surface were converted into higher-valence hydrophilic oxides.

Plasma pre-treatment increased the dissolution of arsenopyrite and pyrite and the dissolution of minerals in aqueous solution was determined according to the oxidation degree of mineral components. Zeta potential determination and FTIR spectroscopic analysis demonstrated that plasma significantly reduced the adsorption of SBX on the surface of the arsenopyrite, which had little effect on the adsorption of SBX on pyrite surface. Plasma modification reduced the floatable pH range of the arsenopyrite and resulted in the adsorption of xanthate on the surface of the arsenopyrite, which was only shown in strongly acidic pulp solution.

It has been demonstrated that low temperature plasmas is expected to achieve efficient separation of sulfide minerals by surface modification. By developing the plasma source for industrial scale material throughputs and researching the atmospheric pressure plasma process, low-temperature plasma might contribute to reduce the dosages of flotation reagents, thereby limiting the hazard of toxic reagents in the beneficiation backwater to the environment.

**Author Contributions:** X.Q., Z.H., Q.L. conceived the project and designed the experiments; J.R. conducted the major experiments and analyzed the data. B.S. performed a part of experiments. All authors participated in writing the manuscript.

**Funding:** This research was funded by the Research Fund Program of Guangdong Provincial Key Laboratory of Development and Comprehensive Utilization of Mineral Resources (Grant No. 2017B030314046).

**Acknowledgments:** We sincerely thank Rongdong Deng and Qicheng Feng for their important guidance in XPS analysis.

**Conflicts of Interest:** The authors declare no conflict of interest.

## Appendix A

**Table A1.** Significance analysis of the effects of input voltage and pre-treatment time on the flotation recovery of arsenopyrite and pyrite.

Input Voltage (V)	<i>p</i> -Value						
	0 min	0.5 min	1 min	2 min	3 min	4 min	5 min
30.00	0.0002	0.0004	0.0002	0.0002	0.0002	<0.0001	<0.0001
35.00	0.0002	<0.0001	<0.0001	<0.0001	0.0001	0.0001	<0.0001
40.00	0.0002	<0.0001	<0.0001	<0.0001	<0.0001	0.0002	<0.0001
45.00	0.0002	0.0001	0.0001	<0.0001	0.0002	<0.0001	0.0002

Note: *p*-value < 0.05 represent a significant effect.

**Table A2.** Significance analysis of the effects of modification temperature on the flotation recovery of arsenopyrite and pyrite.

Significance Analysis				
Temperature (K)	328.50	333.40	342.10	355.40
Input voltage (V)	30.00	35.00	40.00	45.00
<i>p</i> -value	0.0001	0.0019	0.0011	0.0046

**Table A3.** Significance analysis of the effects of plasma modification on the dissolution concentrations of Fe, As and S released from the arsenopyrite.

Significance Analysis ( <i>p</i> -Value)					
Dissolution Time (h)	0.5	1.0	2.0	3.0	5.0
Fe	0.0226	0.0179	0.0376	0.0278	0.0230
As	0.3618	0.8824	0.7957	0.8708	0.9866
S	0.0015	0.0268	0.0277	0.0321	0.0260

**Table A4.** Significance analysis of the effects of plasma modification on the dissolution concentrations of Fe and S released from the pyrite.

Significance Analysis ( <i>p</i> -Value)					
Dissolution Time (h)	0.5	1.0	2.0	3.0	5.0
Fe	0.0057	0.0083	0.0045	0.0177	0.0081
S	0.0103	0.0036	0.0043	0.0102	0.0069

**Table A5.** Significance analysis of the effects of plasma modification on the zeta potential of arsenopyrite in the presence and absence of SBX.

Significance Analysis ( <i>p</i> -Value)											
pH	1.00	2.00	3.00	4.00	5.00	6.00	7.00	8.00	9.00	10.00	11.00
Apy <sup>1</sup>	0.0007	0.0013	0.0092	0.0231	0.0237	0.0392	0.0273	0.0277	0.2913	0.8103	0.5844
Apy-plasma <sup>2</sup>	/	0.0030	0.0195	0.0167	0.5155	0.4564	0.6704	0.5970	0.9003	0.5704	0.5894

<sup>1</sup> Apy represents the bare arsenopyrite; this line of data indicates the statistical significance of the zeta potential of arsenopyrite in the presence and absence of SBX. <sup>2</sup> Apy-plasma represents the plasma-modification arsenopyrite; this line of data indicates the statistical significance of the zeta potential of plasma-modification arsenopyrite in the presence and absence of SBX.

**Table A6.** Significance analysis of the effects of plasma modification on the zeta potential of pyrite in the presence and absence of SBX.

Significance Analysis ( <i>p</i> -Value)										
pH	2.00	3.00	4.00	5.00	6.00	7.00	8.00	9.00	10.00	11.00
Pyrite <sup>1</sup>	0.0002	0.0006	0.0003	0.0271	0.0216	0.0294	0.0327	0.0326	0.0473	0.0665
Pyrite-plasma <sup>2</sup>	0.0001	0.0012	0.0025	0.0334	0.0398	0.0346	0.0320	0.0412	0.5071	0.5293

<sup>1</sup> This line of data indicates the statistical significance of the zeta potential of pyrite in the presence and absence of SBX. <sup>2</sup> This line of data indicates the statistical significance of the zeta potential of plasma-modification arsenopyrite in the presence and absence of SBX.

## References

- Ye, F.P.; Liu, J.T.; Xiong, T.; Xie, M.F. Arsenopyrite removal from pyrite concentrate using pulsating high gradient magnetic separation. *Results Phys.* **2018**, *10*, 822–826. [[CrossRef](#)]
- Hu, N.; Chen, W.; Ding, D.X.; Li, F.; Dai, Z.R.; Li, G.Y.; Wang, Y.D.; Zhang, H.; Lang, T. Role of water contents on microwave roasting of gold bearing high arsenic sulphide concentrate. *Int. J. Miner. Process.* **2017**, *161*, 72–77. [[CrossRef](#)]

3. Valdivieso, A.L.; López, A.A.S.; Escamilla, C.O.; Fuerstenau, M.C. Flotation and depression control of arsenopyrite through pH and pulp redox potential using xanthate as the collector. *Int. J. Miner. Process.* **2006**, *81*, 27–34. [[CrossRef](#)]
4. Tapley, B.; Yan, D. The selective flotation of arsenopyrite from pyrite. *Miner. Eng.* **2003**, *16*, 1217–1220. [[CrossRef](#)]
5. Monte, M.B.M.; Dutra, A.J.B.; Albuquerque, C.R.F., Jr.; Tondo, L.A.; Lins, F.F. The influence of the oxidation state of pyrite and arsenopyrite on the flotation of an auriferous sulphide ore. *Miner. Eng.* **2002**, *15*, 1113–1120. [[CrossRef](#)]
6. Wang, X.H.; Ahlberg, E.; Forssberg, K.S.E. Electrochemical study of surface oxidation and collectorless flotation of arsenopyrite. *J. Appl. Electrochem.* **1992**, *22*, 1095–1103. [[CrossRef](#)]
7. Beattie, M.J.V.; Poling, G.W. A study of the surface oxidation of arsenopyrite using cyclic voltammetry. *Int. J. Miner. Process.* **1987**, *20*, 87–108. [[CrossRef](#)]
8. Urbano, G.; Reyes, V.E.; Veloz, M.A.; González, I.; Cruz, J. Pyrite-arsenopyrite galvanic interaction and electrochemical reactivity. *J. Phys. Chem. C* **2008**, *112*, 10453–10461. [[CrossRef](#)]
9. Chandraprabha, M.N.; Natarajan, K.A.; Somasundaran, P. Selective separation of pyrite from chalcopyrite and arsenopyrite by biomodulation using acidithiobacillus ferrooxidans. *Int. J. Miner. Process.* **2005**, *75*, 113–122. [[CrossRef](#)]
10. Allison, S.A.; Goold, L.A.; Nicol, M.J.; Granville, A. A determination of the products of reaction between various sulphide minerals and aqueous xanthate solution and a correlation of the products with electrode rest potentials. *Metall. Trans.* **1972**, *3*, 2613–2618. [[CrossRef](#)]
11. Sirkeci, A.A. The flotation separation of pyrite from arsenopyrite using hexyl thioethylamine as collector. *Int. J. Miner. Process.* **2000**, *60*, 263–276. [[CrossRef](#)]
12. Monte, M.B.M.; Lins, F.F.; Oliveira, J.F. Selective flotation of gold from pyrite under oxidizing conditions. *Int. J. Miner. Process.* **1997**, *51*, 255–267. [[CrossRef](#)]
13. Moslemi, H.; Gharabaghi, M. A review on electrochemical behavior of pyrite in the froth flotation process. *J. Ind. Eng. Chem.* **2017**, *47*, 1–18. [[CrossRef](#)]
14. Li, Y.Q.; Chen, J.H.; Kang, D.; Guo, J. Depression of pyrite in alkaline medium and its subsequent activation by copper. *Miner. Eng.* **2012**, *26*, 64–69. [[CrossRef](#)]
15. Yang, J.X.; Ding, H.H.; Zhu, Z.; Wang, Q.H.; Wang, J.J.; Xu, J.L.; Chang, X.J. Surface modification of CeO<sub>2</sub> nanoflakes by low temperature plasma treatment to enhance imine yield: Influences of different plasma atmospheres. *Appl. Surf. Sci.* **2018**, *454*, 173–180. [[CrossRef](#)]
16. Kong, F.; Chang, C.; Ma, Y.Y.; Zhang, C.; Ren, C.Y.; Shao, T. Surface modifications of polystyrene and their stability: A comparison of DBD plasma deposition and direct fluorination. *Appl. Surf. Sci.* **2018**, *459*, 300–308. [[CrossRef](#)]
17. Meichsner, J.; Schmidt, M.; Schneider, R.; Wagner, H.E. *Nonthermal Plasma Chemistry and Physics*; CRC Press, Taylor Francis Group: Boca Raton, FL, USA, 2013; Chapters 1.3 and 1.4; pp. 2–5.
18. Bogaerts, A.; Neyts, E.; Gijbels, R.; Mullen, J.V.D. Gas discharge plasmas and their applications. *Spectrochim. Acta Part B* **2002**, *57*, 609–658. [[CrossRef](#)]
19. Ju, Y.G.; Sun, W.T. Plasma assisted combustion: Dynamics and chemistry. *Prog. Energy Combust. Sci.* **2015**, *48*, 21–83. [[CrossRef](#)]
20. Wen, Y.; Shen, C.; Ni, Y.; Tong, S.; Yu, F. Glow discharge plasma in water: A green approach to enhancing ability of chitosan for dye removal. *J. Hazard. Mater.* **2012**, *201*, 162–169. [[CrossRef](#)]
21. May, F.; Gock, E.; Vogt, V.; Brüser, V. Plasma-modification of sulfides for optimizing froth-flotation properties. *Miner. Eng.* **2012**, *35*, 67–74. [[CrossRef](#)]
22. May, F.; Hamann, S.; Quade, A.; Brüser, V. Study on Cu<sub>2</sub>S mineral surface modification by low temperature Ar/O<sub>2</sub> plasmas. *Miner. Eng.* **2013**, *51*, 48–56. [[CrossRef](#)]
23. Hirajima, T.; Mori, M.; Ichikawa, O.; Sasaki, K.; Miki, H.; Farahat, M.; Sawada, M. Selective flotation of chalcopyrite and molybdenite with plasma pretreatment. *Miner. Eng.* **2014**, *66–68*, 102–111. [[CrossRef](#)]
24. May, F.; Hamann, S.; Quade, A.; Brüser, V. Froth flotation improvement by plasma pretreatment of sulfide minerals. *Miner. Eng.* **2017**, *113*, 95–101. [[CrossRef](#)]
25. Feng, Q.C.; Zhao, W.J.; Wen, S.M. Surface modification of malachite with ethanediamine and its effect on sulfidization flotation. *Appl. Surf. Sci.* **2018**, *436*, 823–831. [[CrossRef](#)]
26. Singh, N.; Finch, J.A. Bank profiling and separation efficiency. *Miner. Eng.* **2014**, *66–68*, 191–196. [[CrossRef](#)]

27. Feng, Q.C.; Wen, S.M.; Deng, J.S.; Zhao, W.J. Combined DFT and XPS investigation of enhanced adsorption of sulfide species onto cerussite by surface modification with chloride. *Appl. Surf. Sci.* **2017**, *425*, 8–15. [[CrossRef](#)]
28. Gupta, R.P.; Sen, S.K. Calculation of multiplet structure of core p-vacancy levels. *Phys. Rev. B Condens. Matter* **1974**, *10*, 71–77. [[CrossRef](#)]
29. Nesbitt, H.W.; Muir, I.J.; Prarr, A.R. Oxidation of arsenopyrite by air and air-saturated, distilled water, and implications for mechanism of oxidation. *Geochim. Cosmochim. Acta* **1995**, *59*, 1773–1786. [[CrossRef](#)]
30. Pratt, A.R.; Muir, I.J.; Nesbitt, H.W. X-ray photoelectron and auger electron spectroscopic studies of pyrrhotite and mechanism of air oxidation. *Geochim. Cosmochim. Acta* **1994**, *58*, 827–841. [[CrossRef](#)]
31. Zhu, T.T.; Lu, X.C.; Liu, H.; Li, J.; Zhu, X.Y.; Lu, J.J.; Wang, R.C. Quantitative X-ray photoelectron spectroscopy-based depth profiling of bioleached arsenopyrite surface by *Acidithiobacillus ferrooxidans*. *Geochim. Cosmochim. Acta* **2014**, *127*, 120–139. [[CrossRef](#)]
32. Schaufuss, A.G.; Nesbitt, H.W.; Sciani, M.J.; Hoecsht, H.; Bancroft, M.G.; Szargan, R. Reactivity of surface sites on fractured arsenopyrite (FeAsS) toward oxygen. *Am. Mineral.* **2000**, *85*, 1754–1766. [[CrossRef](#)]
33. Nesbitt, H.W.; Muir, I.J. X-ray photoelectron spectroscopic study of a pristine pyrite surface reacted with water vapour and air. *Geochim. Cosmochim. Acta* **1994**, *58*, 4667–4679. [[CrossRef](#)]
34. Qin, W.Q.; Wang, X.J.; Li, Y.; Ma, L.; Jiao, F.; Liu, R.Z.; Gao, K. Effects of galvanic interaction between galena and pyrite on their flotation in the presence of butyl xanthate. *Trans. Nonferrous Met. Soc.* **2015**, *25*, 3111–3118. [[CrossRef](#)]
35. Asta, M.P.; Cama, J.; Ayora, C.; Acero, P.; Giudici, G.D. Arsenopyrite dissolution rates in O<sub>2</sub>-bearing solutions. *Chem. Geol.* **2010**, *273*, 272–285. [[CrossRef](#)]
36. Feng, Q.C.; Zhao, W.J.; Wen, S.M.; Cao, Q.B. Activation mechanism of lead ions in cassiterite flotation with salicylhydroxamic acid as collector. *Sep. Purif. Technol.* **2017**, *178*, 193–199. [[CrossRef](#)]
37. Feng, Q.C.; Zhao, W.J.; Wen, S.M. Ammonia modification for enhancing adsorption of sulfide species onto malachite surfaces and implications for flotation. *J. Alloys Comp.* **2018**, *744*, 301–309. [[CrossRef](#)]
38. Chanturiya, V.A.; Nedosekina, T.V.; Fedorov, A.A. Separation of pyrite-arsenopyrite products by flotation using low-molecular-weight organic reagents. *J. Min. Sci.* **1998**, *34*, 453–458. [[CrossRef](#)]
39. Zhang, H.; Wang, W.Z.; Li, X.D.; Han, L.; Yan, M.; Zhong, Y.J.; Tu, X. Plasma activation of methane for hydrogen production in a N<sub>2</sub> rotating gliding arc warm plasma: A chemical kinetics study. *Chem. Eng. J.* **2018**, *345*, 67–78. [[CrossRef](#)]
40. Liao, X.Y.; Liu, D.H.; Xiang, Q.S.; Ahn, J.; Chen, S.G.; Ye, X.Q.; Ding, T. Inactivation mechanisms of non-thermal plasma on microbes: A review. *Food Control* **2017**, *75*, 83–91. [[CrossRef](#)]
41. Corkhill, C.L.; Vaughan, D.J. Arsenopyrite oxidation—A review. *Appl. Geochem.* **2009**, *24*, 2342–2361. [[CrossRef](#)]
42. Ruiz-Agudo, E.; Putnis, C.V.; Putnis, A. Coupled dissolution and precipitation at mineral-fluid interfaces. *Chem. Geol.* **2014**, *383*, 132–146. [[CrossRef](#)]

